Current Biology, Vol. 15, 828–832, May 10, 2005, ©2005 Elsevier Ltd All rights reserved. DOI 10.1016/j.cub.2005.03.019

Efficient Chromosome Capture Requires a Bias in the 'Search-and-Capture' Process during Mitotic-Spindle Assembly

R. Wollman,[1] E.N. Cytrynbaum,[2] J.T. Jones,[3] T. Meyer,[3] J.M. Scholey,[1] and A. Mogilner[1,4,*]
[1]Laboratory of Cell and Computational Biology
Center for Genetics and Development
University of California, Davis
Davis, California 95616
[2]Department of Mathematics
University of British Columbia
Vancouver, British Columbia
Canada V6T 1Z2
[3]Department of Molecular Pharmacology
Stanford University Medical Center
Stanford, California 94305
[4]Department of Mathematics
University of California, Davis
Davis, California 95616

Summary

The mitotic spindle assembles into a bipolar, microtubule-based protein machine during prometaphase. One proposed mechanism for this process is "search-and-capture," in which dynamically unstable microtubules (MTs) search space to capture chromosomes [1]. Although existing theoretical estimates [2, 3] suggest that dynamic instability is efficient enough to allow capture within characteristic mitotic timescales, they are limited in scope and do not address the capture times for realistic numbers of chromosomes. Here we used mathematical modeling to explore this issue. We show that without any bias toward the chromosomes, search-and-capture is not efficient enough to explain the typical observed duration of prometaphase. We further analyze search-and-capture in the presence of a spatial gradient of a stabilizing factor [4–6] that biases MT dynamics toward the chromosomes. We show theoretically that such biased search-and-capture is efficient enough to account for chromosome capture. We also show that additional factors must contribute to accelerate the spindle assembly for cells with large nuclear volumes. We discuss the possibility that a RanGTP gradient introduces a spatial bias into microtubule dynamics and thus improves the efficiency of search-and-capture as a mechanism for spindle assembly.

Results

Optimal Unbiased 'Search and Capture' Is Not Fast Enough to Account for Observed Rates of Spindle Assembly

Before chromatid segregation can occur, a bipolar mitotic spindle consisting of two overlapping microtubules (MTs) arrays must assemble [1]. Some of these MTs attach to the kinetochores. According to the search-and-capture model [1], MTs nucleate in a random direction and grow and shrink dynamically to probe space and eventually encounter target kinetochores. Theoretical analysis of the search-and-capture model showed that MT dynamic instability is very effective if it is regulated so that the rescue frequency is close to zero (i.e., MTs do not search repeatedly in the "wrong" direction) while the catastrophe frequency is such that a MT grows on average to a length equal to the mean pole-kinetochore distance (i.e., MTs neither undergo premature catastrophe when growing in the "right" direction nor "waste time" growing in the "wrong" direction) [2, 3]. This analysis is consistent with the measured decrease in rescue frequency from 0.175 s^{-1} in interphase to 0.023 s^{-1} in prometaphase [7].

The estimates in [2] do not analyze the capture times for a realistic geometry or number of chromosomes. In the Supplemental Data available with this article online, we describe mathematical analysis and Monte Carlo simulations that estimate the time to capture *for multiple chromosomes*. In short, the computer code places a number of chromosomes at random locations inside a nuclear sphere, 10 μm in radius (Figure 1). Sister kinetochores lie back-to-back—that is, the capture surfaces of partner kinetochores face in opposite directions [8]—so we assume that each kinetochore can be reached by MTs emanating from one pole only. For each kinetochore, we calculate the probability of capture if one assumes that MTs are nucleated in random directions and their dynamic properties are spatially independent (Figure 1C). We then use a random number generator to simulate the number of unsuccessful searches before the chosen kinetochore is captured and find the time to capture. We repeat this procedure for all kinetochores and find the maximal time to capture the final unattached kinetochore. Values of the model parameters are listed in Table S1 in the Supplemental Data.

To test the model, we first examined the simplified case of a single aster containing 250 MTs and searched for a single target at a distance of 10 μm. Our numerical analysis yielded a mean time to capture of 23 min, similar to previous results [2]. We further tested whether the capture of multiple chromosomes can occur in a reasonable biological timescale under the same modeling assumptions. We first calculated the optimal catastrophe frequency (0.0134 s^{-1}) by minimizing the search time and assuming a uniform distribution of chromosomes in the nucleus. Then, using the optimal conditions, we simulated the unbiased model with 46 chromosomes.

Calculated mean times to capture are 511 min and 125 min for 250 and 1000 searching MTs, respectively (Figures 2E and 2F). This time is much longer than the time it takes to capture a single kinetochore because the process of capturing a kinetochore is stochastic, with significant variations. In the case of multiple chromosomes, the process ends only when the last kinetochore is captured, so the most "unsuccessful" and prolonged search determines the time it takes to capture the kinetochore. In fact, the mean time to search

*Correspondence: mogilner@math.ucdavis.edu

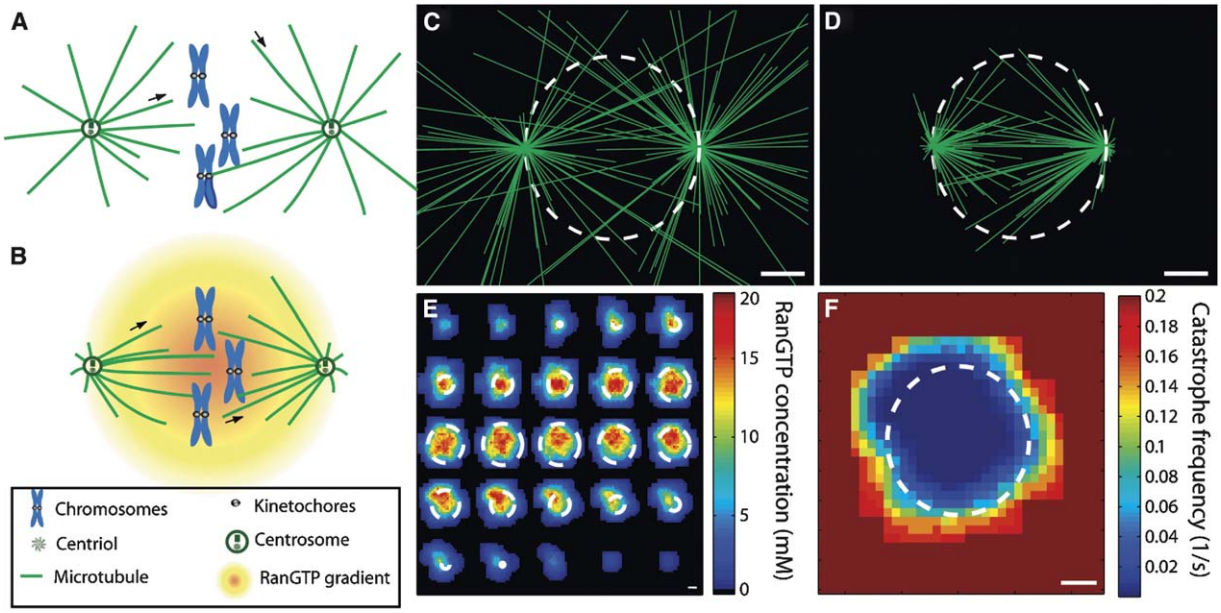

Figure 1. Biased and Unbiased Search and Capture

Schematic of the unbiased (A) and RanGTP-biased (B) search-and-capture models and graphical representation of stochastic simulations. 2-D projection of 3-D simulation of MT dynamics in the unbiased (C) and biased (D) models. MT distribution for the unbiased model (C) was generated with spatially homogeneous optimal catastrophe frequency. Spatially dependent catastrophe frequency for the biased model (in the middle nuclear cross-section) is shown in panel (F). The catastrophe frequency was calculated based on the assumption that it is an exponentially decaying function of the RanGTP concentration with a chemical scale of 10 μM and a value of 0.2 catastrophes per second in the absence of RanGTP. The 3-D distribution of the RanGTP gradient (serial sections in [E]) was calculated based on the assumption of a uniform distribution of chromosomes in the nucleus and linear superposition of exponentially decaying RanGTP gradients centered at each chromosome. The dashed white line represents the position of the nuclear envelope before NEB. Scale bars represent 5 μm.

is a logarithmic function of the number of the chromosomes (Figure 3B). (See Equation S17 in the Supplemental Data.)

The search time clearly decreases as the number of MTs increases (Figure 2F). Even with 1000 searching MTs, which is an upper limit to the usual estimate of hundreds of MTs, the mean estimated time until capture of 46 chromosomes in the unbiased model is substantially greater than experimental measurements (20–30 min; see Figure S2). Thus, even under optimal conditions, the unbiased model cannot explain the experimental results.

Biased Search and Capture Is Sufficiently Fast to Account for Observed Rates of Mitosis

The MT catastrophe frequency was never measured in the vicinity of chromosomes in vivo, although astral MTs were found to display a catastrophe frequency of 0.075 s^{-1} away from the spindle during prometaphase [7]. This value is 5.6-fold larger than the calculated optimal value of 0.0134 s^{-1}, and simulations show that it would yield an unrealistic mean capture time of 3720 min. This suggests that there is a bias of MT dynamics near the chromosome, such that a MT growing in the "wrong" direction would collapse rapidly, whereas a MT that is close to the target would be allowed to continue its growth. We tested whether such a bias can increase the efficiency of search and capture to reach biologically observed time scales. Although there are several molecular mechanisms that could plausibly generate such a bias in MT dynamics, here we examine the possibility that a RanGTP gradient could serve to stabilize MTs in the vicinity of chromosomes, as was previously suggested [4, 5, 9–13]. To explore this possibility quantitatively, we simulated the following model.

We calculated the spatial distribution of RanGTP in a gradient decreasing away from the chromosomes (Supplemental Data and Figures 1B and 1E). We made the catastrophe frequency a decreasing function of RanGTP concentration, so that MTs undergo catastrophe very rapidly away from the nucleus and are very stable near the chromosomes. We found that the search durations were minimized under conditions in which RanGTP decreased rapidly away from the nucleus but not rapidly enough to change much between the adjacent chromosomes. In such cases there exists a "stabilizing sphere" of radius similar to that of the nucleus, such that the catastrophe frequency is step-like (Figure 1F) with no catastrophes inside the nucleus and a high frequency of catastrophes outside the nucleus.

We simulated this optimal, simplified, biased model, in which a MT underwent a catastrophe immediately outside the nuclear sphere and did not catastrophe inside it (Figure 1D). (Other than that, the simulations were as described above; see also the Supplemental Data.) The results are shown in Figures 2A and 2B. The mean time until capture became as short as 11–48 min for 1000–250 searching MTs, respectively. This result is

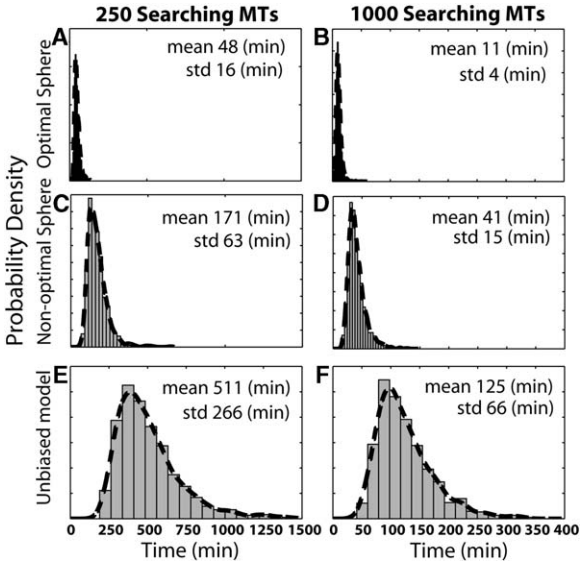

Figure 2. Distribution of Time until Capture

Simulation results summarized as the distribution of time until capture under different assumptions: stabilizing sphere with radius of the nucleus (top: [A and B]), stabilizing sphere with radius of 1.5 times the nuclear radius (middle: [C and D]), and an unbiased model with optimal dynamic instability parameters (bottom: [E and F]). Each model is presented both for 250 searching MTs (left: [A, C, and E]) and 1000 searching MTs (right: [B, D, and F]). Bars are histograms of 1000 simulations, and the dashed line is an estimate of the probability density function obtained from average shifted histograms.

an order of magnitude faster than in the unbiased model because in this case the MTs do not spend time growing in the "wrong" direction and do not grow too long because they are destabilized away from the chromosomes (Supplemental Data). The estimated time compares well with the measured prometaphase duration of 20–30 min (Figure S2), demonstrating that introducing a bias into the catastrophe frequency, with MTs being more stable proximal to the chromosomes and less stable distally, can explain the observed duration of prometaphase.

Our analysis shows that the average search time is inversely proportional to the number of MTs (Equations S17 and S19). Not surprisingly, the cell increases the number of MTs as it enters mitosis. The time also decreases drastically when the size of the kinetochores is increased [7]. We performed simulations for 15 different effective kinetochore radii from 0.08 to 1.2 μm and for 20 different numbers of searching MTs from 100 to 2000. Each set of parameters was averaged from 100 simulations, equating to a total of 30,000 simulations. Figure 3A shows how the search time depends on the kinetochore size and MT number and demonstrates that the biased-search parameters have to be finely tuned to achieve the observed capture time. On the other hand, our analysis predicts that the search time depends weakly, as a logarithmic function, on chromosome number (Figure 3B). Moreover, we predict that the variance of the search time is proportional to the logarithm of the number of chromosomes.

The size of the stabilizing sphere is another important parameter to be regulated. The stabilizing sphere should include all the chromosomes as well as the path between them and the centrosomes, but if it becomes too big, the search-and-capture process loses its efficiency because MTs grow too long and sometimes in the "wrong" direction. We ran the simulation for a sphere with a radius 1.5 times larger than the nuclear radius and observed that the mean time until capture increased 4-fold (Figures 2C and 2D).

An important parameter of our model is spindle size, implemented as the nuclear radius. Previous work [2] showed that the average time of the unbiased search and capture grows exponentially with increasing chromosome-to-pole distance for a single chromosome. Our numerical simulations confirm that, in the unbiased model for multiple chromosomes, the search time is an exponential function of the nuclear size (Figure 3C). In the biased model, according to both analysis and simulations (Figure 3C), the search time increases more slowly as a cubic function of the radius, which makes it orders of magnitude more efficient. However, both models predict an average search time that is larger than characteristic biological time scales for nuclei of 15 μm radius or greater; for the unbiased model, the average predicted time is approximately 10 hr, and for the biased model it is approximately 1 hr.

Prometaphase Is Prolonged by 2- to 3-fold in Hela Cells with Perturbed Levels of Ran

We measured the prometaphase duration approximately 20 min in Hela cells (Supplemental Data). An obvious and testable prediction of our models is that perturbations of the RanGTP gradient should increase both the time to capture and the duration of prometaphase, provided that this gradient affects the MT dynamics as assumed in the model. Our model predicts that a dominant-negative mutant, RanL43E, will reduce the efficiency of any stabilizing gradient and thereby increase prometaphase duration, whereas a constitutively active mutant, RanQ69L, should increase the size of the stabilizing sphere and thereby overstabilize MTs and increase the duration of prometaphase. To test this prediction, we perturbed the RanGTP system in Hela cells constitutively expressing a mitosis biosensor by transfecting them with sequences encoding three different forms of Ran. Specifically, we overexpressed native Ran and introduced a dominant-negative Ran construct as well as a constituently active one [14]. Both constituently active and dominant-negative constructs caused a 2- to 3-fold increase in prometaphase duration (Supplemental Data, including Figures S1 and S2), as predicted, indicating that a RanGTP gradient can act as bias generator in the search-and-capture process.

Discussion

Our work demonstrates that without any bias, the search-and-capture mechanism is inefficient except in very small cells. Furthermore, due to the polynomial increase in search time with nuclear size, biased search and capture could not be the sole mechanism for spindle assembly in large cells. This demonstrates the limi-

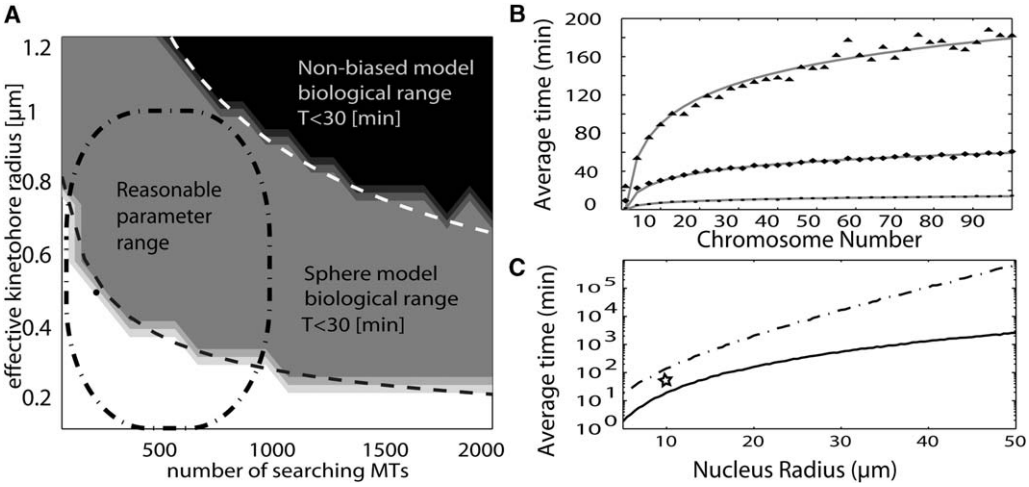

Figure 3. Time-to-Capture Dependence on the Model Parameter Values

(A) Results from a parameter scan of effective kinetochore radius from 0.08 (μm) to 1.2 (μm) and number of searching MTs from 100 to 2000. Black region: The average time until capture for both biased and unbiased models is smaller than 30 min. Gray region: The average time until capture is smaller than 30 min only for the biased model. White region: The average time until capture for both models is greater than 30 min. Dashed lines are analytical (radius is inversely proportional to square root of MT number) fits to the stochastic simulations based on Equation S20 in the Supplemental Data. The dash-and-dot circle represents an order-of-magnitude estimate of reasonable biological range. A black dot marks the parameter choice made by Holy and Leibler [2].

(B) The effect of chromosome number on time until capture. Average time until capture with different numbers of chromosomes under three different models: unbiased model with 1000 searching MTs (triangles), biased model with 250 searching MTs (diamonds), and biased model with 1000 searching MTs (circles). Each data point is the average time until capture from 200 simulations. Gray lines are analytical (logarithmic function) fits to the stochastic simulations based on Equations S17 and S19.

(C) The unbiased (dot-and-dash) model shows exponential increase of the time to capture as a function of nuclear radius. In the biased (solid) model, the time is proportional to the cube of the radius. A typical experimental observation (nuclear radius and prometaphase time), such as that illustrated in the Figure S1, is shown with the star.

tation of the centrosomal assembly pathway and supports experimental evidence that centrosomal and chromosomal spindle assembly pathways are not mutually exclusive [15–17].

Our analysis predicts that the search time depends weakly, as a logarithmic function, on chromosome number. This implies that the time it takes to capture all chromosomes is not sensitive to mutations changing the number of chromosomes. This may have implications for cancer, in which genomic instability often causes an increase in chromosome number [18]. The logarithmic dependency on chromosome number means there is only a 20% increase in the average time it takes to capture chromosomes when the number of chromosomes increases by 10, suggesting that cancer cells pay a very small price for their genomic instability. Moreover, we predict that the stochastic fluctuations (variance/mean) of the search time are independent of the number of chromosomes.

It is tempting to speculate that the cell optimizes not just the rescue and catastrophe frequencies [2] but also the size of the kinetochores [8] and a number of other parameters to decrease the duration of prometaphase. According to our analysis, larger kinetochores reduce the time required for capture, and centrosome-independent kinetochore fiber formation could effectively increase the kinetochore size [19, 20]. In any event, the cell must strike a balance between hiding and exposing the kinetochores, a balance that minimizes kinetochore misorientation, e.g., merotelic or syntelic attachment, and yet permits effective capture.

Our computer models are based on a number of simplifying assumptions that may affect the validity of the results. In the model, any one chromosome-capture event is independent of any other; there is no steric interference between the kinetochores. Such interference would increase the time to capture because some chromosomes would be "hidden" from view until other chromosomes were captured. It is not clear how poleward movements of mono-oriented chromosomes would affect the time it takes to capture the sister chromatid. Also, molecular details of MT-kinetochore or MT-chromosome-arm interactions may affect our estimates if reaching the target does not always lead to kinetochore attachment, or if lateral kinetochore attachments to the wall of the MT polymer lattice are frequent. Our analysis also assumes a purely centrosome-directed spindle-assembly pathway. This may not be the case [20, 21]: MT nucleation near the chromosomes as well as on the centrosomes, and the crosslinking between those differently nucleating MTs, might drastically decrease the duration of bipolar spindle assembly.

Finally, our experimental results are merely an indication that the RanGTP gradient may contribute to the bias. Modeling of the RanGTP gradient [22] suggests that it may not be possible to generate such a gradient in human somatic cells. Moreover, mutations in the Ran effector RCC1 in mammalian tissue culture cells show little change in spindle morphology [23], unlike the response seen in *Xenopus* extract spindles, suggesting that a RanGTP gradient may have mitotic roles in some, but not all systems. Another possibility is that RanGTP

affects MT-kinetochore interactions rather than MT dynamics [24]. Also, chemicals other than Ran [25, 26] could contribute to the bias in search and capture, and there may exist other, as-yet-undiscovered, mechanisms for chromosomes or kinetochores to influence MT dynamics. Further combined experiments and computer simulations of prometaphase in model organisms will lead to an improved understanding of the chemically biased search-and-capture mechanism.

Supplemental Data

Supplemental Data are available with this article online at http://www.current-biology.com/cgi/content/full/15/9/828/DC1/.

Acknowledgments

R.W., E.C., J.S., and A.M. are supported by National Institutes of Health grants GM-55507 and GM-068952. J.J. and T.M. are supported by National Institutes of Health grant MH6481. We thank Dr. Won Do Heo for his gift of the Ran constructs.

Received: December 15, 2004
Revised: February 4, 2005
Accepted: March 3, 2005
Published online: March 17, 2005

References

1. Kirschner, M., and Mitchison, T. (1986). Beyond self-assembly: From microtubules to morphogenesis. Cell *45*, 329–342.
2. Holy, T.E., and Leibler, S. (1994). Dynamic instability of microtubules as an efficient way to search in space. Proc. Natl. Acad. Sci. USA *91*, 5682–5685.
3. Hill, T.L. (1985). Theoretical problems related to the attachment of microtubules to kinetochores. Proc. Natl. Acad. Sci. USA *82*, 4404–4408.
4. Carazo-Salas, R.E., Gruss, O.J., Mattaj, I.W., and Karsenti, E. (2001). Ran-GTP coordinates regulation of microtubule nucleation and dynamics during mitotic-spindle assembly. Nat. Cell Biol. *3*, 228–234.
5. Kalab, P., Pu, R.T., and Dasso, M. (1999). The ran GTPase regulates mitotic spindle assembly. Curr. Biol. *9*, 481–484.
6. Askjaer, P., Galy, V., Hannak, E., and Mattaj, I.W. (2002). Ran GTPase cycle and importins alpha and beta are essential for spindle formation and nuclear envelope assembly in living Caenorhabditis elegans embryos. Mol. Biol. Cell *13*, 4355–4370.
7. Rusan, N.M., Tulu, U.S., Fagerstrom, C., and Wadsworth, P. (2002). Reorganization of the microtubule array in prophase/prometaphase requires cytoplasmic dynein-dependent microtubule transport. J. Cell Biol. *158*, 997–1003.
8. Nicklas, R.B., and Ward, S.C. (1994). Elements of error correction in mitosis: Microtubule capture, release, and tension. J. Cell Biol. *126*, 1241–1253.
9. Wilde, A., Lizarraga, S.B., Zhang, L., Wiese, C., Gliksman, N.R., Walczak, C.E., and Zheng, Y. (2001). Ran stimulates spindle assembly by altering microtubule dynamics and the balance of motor activities. Nat. Cell Biol. *3*, 221–227.
10. Wilde, A., and Zheng, Y. (1999). Stimulation of microtubule aster formation and spindle assembly by the small GTPase Ran. Science *284*, 1359–1362.
11. Ohba, T., Nakamura, M., Nishitani, H., and Nishimoto, T. (1999). Self-organization of microtubule asters induced in Xenopus egg extracts by GTP-bound Ran. Science *284*, 1356–1358.
12. Carazo-Salas, R.E., and Karsenti, E. (2003). Long-range communication between chromatin and microtubules in Xenopus egg extracts. Curr. Biol. *13*, 1728–1733.
13. Li, H.Y., Wirtz, D., and Zheng, Y. (2003). A mechanism of coupling RCC1 mobility to RanGTP production on the chromatin in vivo. J. Cell Biol. *160*, 635–644.
14. Heald, R., and Weis, K. (2000). Spindles get the ran around. Trends Cell Biol. *10*, 1–4.
15. Tulu, U.S., Rusan, N.M., and Wadsworth, P. (2003). Peripheral, non-centrosome-associated microtubules contribute to spindle formation in centrosome-containing cells. Curr. Biol. *13*, 1894–1899.
16. Rebollo, E., Llamazares, S., Reina, J., and Gonzalez, C. (2004). Contribution of noncentrosomal microtubules to spindle assembly in Drosophila spermatocytes. PLoS Biol. *2*, E8.
17. Wadsworth, P., and Khodjakov, A. (2004). E pluribus unum: Towards a universal mechanism for spindle assembly. Trends Cell Biol. *14*, 413–419.
18. Bharadwaj, R., and Yu, H. (2004). The spindle checkpoint, aneuploidy, and cancer. Oncogene *23*, 2016–2027.
19. Khodjakov, A., Copenagle, L., Gordon, M.B., Compton, D.A., and Kapoor, T.M. (2003). Minus-end capture of preformed kinetochore fibers contributes to spindle morphogenesis. J. Cell Biol. *160*, 671–683.
20. Maiato, H., Rieder, C.L., and Khodjakov, A. (2004). Kinetochore-driven formation of kinetochore fibers contributes to spindle assembly during animal mitosis. J. Cell Biol. *167*, 831–840.
21. Gruss, O.J., Wittmann, M., Yokoyama, H., Pepperkok, R., Kufer, T., Sillje, H., Karsenti, E., Mattaj, I.W., and Vernos, I. (2002). Chromosome-induced microtubule assembly mediated by TPX2 is required for spindle formation in HeLa cells. Nat. Cell Biol. *4*, 871–879.
22. Gorlich, D., Seewald, M.J., and Ribbeck, K. (2003). Characterization of Ran-driven cargo transport and the RanGTPase system by kinetic measurements and computer simulation. EMBO J. *22*, 1088–1100.
23. Li, H.Y., and Zheng, Y. (2004). Phosphorylation of RCC1 in mitosis is essential for producing a high RanGTP concentration on chromosomes and for spindle assembly in mammalian cells. Genes Dev. *18*, 512–527.
24. Dasso, M. (2002). The Ran GTPase: Theme and variations. Curr. Biol. *12*, R502–R508.
25. Andersen, S.S., Ashford, A.J., Tournebize, R., Gavet, O., Sobel, A., Hyman, A.A., and Karsenti, E. (1997). Mitotic chromatin regulates phosphorylation of Stathmin/Op18. Nature *389*, 640–643.
26. Sampath, S.C., Ohi, R., Leismann, O., Salic, A., Pozniakovski, A., and Funabiki, H. (2004). The chromosomal passenger complex is required for chromatin-induced microtubule stabilization and spindle assembly. Cell *118*, 187–202.

Efficient Chromosome Capture Requires a Bias in the 'Search-and-Capture' Process during Mitotic-Spindle Assembly

R. Wollman, E.N. Cytrynbaum, J.T. Jones, T. Meyer, J.M. Scholey, and A. Mogilner

Mathematical and Experimental Analysis of the 'Search-and-Capture' Process

Here we report on the results of mathematical analyses and computer simulations that support the statements and claims made in the main text for both the unbiased and the biased models. The supplemental material is organized as follows. First, we describe the mathematical analysis of the unbiased model. We derive a formula for the average search time of one MT searching for one kinetochore, then find the optimal value of the catastrophe frequency minimizing the search time, and finally generalize the results to arbitrary numbers of MTs and kinetochores. Second, we expand the analysis to the unbiased model. Third, we investigate the dependence of the search time on the model parameters and compare the biased and unbiased searches. Fourth, we describe three computer simulations, including one simulation of the unbiased model and two variants of the biased model. Finally, we describe the experimental and theoretical procedures and experimental results. The model parameters are listed in the table.

Derivation of the Probability Distribution for the Search Time in the Unbiased Model

I. One MT and one kinetochore

(1) Let us define (i) the probability that a kinetochore (kt) is eventually captured by a MT in the presence of a single MT nucleation site before time τ as $P(t \leq \tau)$, where t denotes the time of capture, (ii) the probability of having n sequentially nucleated MTs fail to capture the kinetochore as $P(n)$, and (iii) the probability that, when the $(n+1)$st MT captures the kinetochore, the time used up by the preceding n cycles is less than τ as $P(t \leq \tau|n)$. According to the law of total probability [S1], we can decompose $P(t \leq \tau)$ into a sum over n as follows:

$$P(t \leq \tau) = \sum_{n=0}^{\infty} P(t \leq \tau|n) \cdot P(n) \tag{S1}$$

We analyze each of the component probabilities in more detail, starting with $P(n)$ and continuing with $P(t \leq \tau|n)$.

(2) Each time a MT nucleates, it has some probability p to attach to a kinetochore, which is at distance x from the centrosome. This probability can be decomposed into the product of (i) the probability of nucleating in the right direction ($P_{direction}$) and (ii) the probability of not undergoing catastrophe before the kinetochore is reached ($P_{no\ cat}$).

The probability of nucleating in the right direction: If MTs are nucleated and grow in random, unbiased directions, then the probability of nucleating in the right direction can be calculated as the solid angle subtended at the origin (centrosome) by the kinetochore "target" surface area divided by the total solid angle 4π [S2]. This ratio can be expressed in terms of the ratio of the kinetochore target area to the total area of the surface of a sphere of radius x:

$$P_{direction} = \frac{\pi r_{kt}^2}{4\pi x^2} = \frac{r_{kt}^2}{4x^2}, \tag{S2}$$

where r_{kt} is the effective kinetochore radius.

Probability of not undergoing catastrophe before the kinetochore is reached: The time from the nucleation of a MT to its catastrophe is approximately an exponential random variable [S3]: the corresponding probability density function is $f_{cat}\exp[-f_{cat}t]$, where f_{cat} is the catastrophe frequency. The probability that a MT nucleated at the proper angle reaches the kinetochore is the probability that the MT does not catastrophe before the "success" time $T_s = x/V_g$, the time required to grow at a rate V_g to a length x equal to the distance to the kinetochore, so

$$P_{no\ cat}\ (t < T_s) = \int_{T_s}^{\infty} f_{cat}\exp[-f_{cat}t]dt = \exp[-f_{cat}x/V_g]. \tag{S3}$$

Therefore, the probability that a MT will reach a kinetochore is

$$p = P_{direction}P_{no\ cat} = \frac{r_{kt}^2}{4x^2} \cdot \exp\left[-\frac{xf_{cat}}{V_g}\right]. \tag{S4}$$

(3) The average unsuccessful cycle time (the lifespan of an unsuccessful MT from nucleation through catastrophe to complete depolymerization) T_{uc} is the average time until a catastrophe, $(1/f_{cat})$, plus the corresponding time for the MT to shrink, (V_g/V_sf_{cat}):

$$T_{uc} = \frac{V_g + V_s}{V_sf_{cat}}, \tag{S5}$$

where V_s is the rate of MT shrinking.

(4) The number of unsuccessful nucleations required before a successful MT-kinetochore attachment is a geometric random variable [S1]: $P(n) = p(1-p)^n$. The conditional probability $P(t < \tau|n)$ equals the probability that the total time taken up by n unsuccessful searches is less than τ:

$$P(t \leq \tau|n) = P\left(\sum_{i=1}^{n} T_{cycle,i} < \tau\right). \tag{S6}$$

The duration of each nucleation cycle, given that the rescue frequency is zero, is an exponential random variable with the average time T_{uc} calculated above. The sum of n exponential random variables is the Gamma random variable [S1]

$$P(t \leq \tau|n) = \frac{1}{T_{uc}^n(n-1)!}\int_0^{\tau} s^{n-1}e^{-s/T_{uc}}ds. \tag{S7}$$

Finally, the probability for a capture event occurring

before time τ is:

$$\begin{aligned} P(t \le \tau) &= p + \sum_{n=1}^{\infty}[(1-p)^n\, p \cdot P(t \le \tau' | n)] \\ &= p + \sum_{n=1}^{\infty}\left[(1-p)^n\, p \cdot \frac{1}{T_{uc}^n (n-1)!}\int_0^{\tau} s^{n-1} e^{-s/T_{uc}} ds\right] \\ &= p + \frac{p(1-p)}{T_{uc}}\int_0^{\tau'}\left[\sum_{n=1}^{\infty}\frac{(1-p)^n s^n}{T_{uc}^n n!}\, e^{-s/T_{uc}}\right] ds \\ &= p + \frac{p(1-p)}{T_{uc}}\int_0^{\tau'} e^{-ps/T_{uc}} ds \\ &= p + (1-p)(1 - e^{-p\tau'/T_{uc}}) \end{aligned} \tag{S8}$$

where $\tau > x/V_g$ and $\tau' = \tau - x/V_g$. For values of $p \ll 1$, the characteristic number of unsuccessful searches is $n \gg 1$ and the typical search time is $\tau \gg x/V_g$, so

$$P(t \le \tau) \approx 1 - e^{-p\tau/T_{uc}} \tag{S9}$$

This analysis shows that the time until capture is distributed exponentially with the approximate average search time:

$$T_{search}^{1,1} = \frac{T_{uc}}{p} = \frac{V_g + V_s 4x^2}{V_s f_{cat}\; r_{kt}^{\,2}} \cdot \exp\left[\frac{x f_{cat}}{V_g}\right]. \tag{S10}$$

where $T_{search}^{i,j}$ is the search time of i MTs searching for j targets.

II. Optimal catastrophe frequency

One can find the optimal catastrophe frequency by taking the derivative of Equation S10:

$$\begin{aligned} \frac{d}{df_{cat}}\left(\exp\left[\frac{x f_{cat}}{V_g}\right]/f_{cat}\right) &= \left(\exp\left[\frac{x f_{cat}}{V_g}\right]/f_{cat}^2\right)\cdot\left(\frac{x f_{cat}}{V_g} - 1\right) \\ &= 0,\; f_{cat}^{optimal} = \frac{V_g}{x} \end{aligned} \tag{S11}$$

This result was obtained previously by Holy and Leibler [S4], although by less rigorous means.

III. N_M MT and one kinetochore

Let N_M be the number of searching MTs. For simplicity, we analyze both biased and unbiased models while assuming that the MT number is constant. In fact, this number fluctuates because MT nucleation is a stochastic process. However, because both models are analyzed under optimal conditions, we assume a high nucleation rate such that the number of nucleation sites is the limiting factor.

The probability that at least one MT will attach to the target before time τ is

$$\begin{aligned} P_{NM,1}(t \le \tau) &= 1 - P_{NM,1}(t > \tau) = 1 - (P(t > \tau))^{N_M} \\ &= 1 - (e^{-p\tau/T_{uc}})^{N_M} = 1 - e^{-p\tau N_M/T_{uc}}. \end{aligned} \tag{S12}$$

Therefore, the time until capture of a single kinetochore by N_M MTs distributes exponentially as well with the average search time:

$$T_{search}^{N_M,1} = \frac{T_{uc}}{N_M p} = \frac{V_g + V_s}{V_s f_{cat}}\frac{4x^2}{N_M r_{kt}^2} \cdot \exp\left[\frac{x f_{cat}}{V_g}\right], \tag{S13}$$

which is N_M times less than that for one MT.

IV. N_M MTs and N_K kinetochores

Let N_K be the number of kinetochores. Because the attachment of a kinetochore is independent of all other kinetochore attachments, the probability that all kinetochores will be attached to MTs before time τ is

$$\begin{aligned} P_{NM,NK}(t \le \tau) &= (P_{NM,1}(t \le \tau))^{N_K} \\ &= (1 - e^{-p\tau N_M/T_{uc}})^{N_K}. \end{aligned} \tag{S14}$$

The corresponding probability density function can be found by differentiation:

$$\begin{aligned} f(t) &= \frac{d}{dt}\,(1 - e^{-ptN_M/T_{uc}})^{N_K} \\ &= \frac{pN_K N_M}{T}\,(1 - e^{-ptN_M/T_{uc}})^{N_K - 1}\, e^{-ptN_M/T_{uc}} \end{aligned} \tag{S15}$$

The maximum of this probability density function can be found by differentiation:

$$\begin{aligned} \frac{d}{dt} f(t) = \frac{pN_K N_M}{T_{uc}}\,(1 - e^{-ptN_M/T_{uc}})^{N_K - 2}\left(\frac{d}{dt}\, e^{-ptN_M/T_{uc}}\right) \\ \cdot\,[1 - N_K e^{-ptN_M/T_{uc}}] = 0. \end{aligned} \tag{S16}$$

Solving this equation (the expression in square brackets is equal to zero), we find the most likely time when the last kinetochore is captured, $t = (T_{uc}/pN_M)\ln N_K$. The *average* time to capture is not equal to the most likely time, but numerical analysis shows that these two times are very close. Therefore, the average time necessary for the attachment of all kinetochores is

$$\begin{aligned} T_{search}^{N_M,N_K} = \frac{T_{uc}}{pN_M} \cdot \ln N_K = C\frac{V_g + V_s}{V_s f_{cat}}\frac{4x^2}{N_M r_{kt}^2} \\ \cdot \exp\left[\frac{x f_{cat}}{V_g}\right] \cdot \ln N_K,\; C \sim 1 \end{aligned} \tag{S17}$$

Numerical analysis shows that, remarkably, the standard deviation of the search time σ is almost independent of the kinetochore number when this number is greater than 10:

$$\sigma \approx 1.3 \cdot (T_{uc}/pN_M) \sim T_{search}^{N_M,N_K}/\ln N_K. \tag{S18}$$

This formula suggests an interesting test of the theory: if we know the average measured search time, we can divide it by the logarithm of the chromosome number, find the standard deviation of the search time and compare it with the measured value. Jones et al. [S5] measured the time of mitosis as 32 $\pm$ 6 min; prometaphase takes about half of this time. 32 min/(ln(92 kts)) $\approx$ 7 min, which is in a very good agreement with the measured value.

Derivation of the Probability Distribution for the Search Time in the Biased Model

(1) In the biased model, the time to catastrophe is not an exponential random variable, so the analytical approach provides only limited results. However, we can use Wald's theorem [S1] to calculate the average time it takes to capture a single kinetochore. This theorem states that the average value of the sum of a random number, n,

of identically distributed random variables is equal to the product of the mean of the number of variables and the mean of the distribution of the variables:

$$\left\langle \sum_{i=1}^{n} T_i \right\rangle = \langle n \rangle \cdot \langle T_i \rangle.$$

In our case, n is the number of unsuccessful searches, and T_i is the i^{th} cycle time, so we have $\langle n \rangle = 1/p$ and $\langle T_i \rangle = T_{uc}$. The theorem says that the average time to capture $T^{1,1}_{search} = T_{uc}/p$. Here, as in the unbiased model, the meaning of the variables T_{uc} and p are the same, i.e., the average time of an unsuccessful search cycle and the probability to capture respectively, but their values are different, as discussed below. When the number of MTs is N_M, similar simple argument shows that the average time to capture

$$T^{N_M,1}_{search} = T_{uc}/(N_M p).$$

(2) In the biased model, the time of an unsuccessful search T_{uc} is less random than in the unbiased model (see below). Because of that, the following heuristic argument allows us to estimate the probability distribution, as well as the average and standard deviation of the time to capture, in the biased model when the kinetochore number is greater than 1. In this case, the random number of unsuccessful searches n before capture is related to the time to capture t by the expression $n \approx t/T_{uc}$. Because n is a geometric random variable, $P(n) = p(1-p)^n$, so $f(t) \approx P(t/T_{uc}) = p(1-p)^{t/T_{uc}} = pe^{-\alpha t}$. Here $\alpha = -\ln(1-p)/T_{uc} \approx p/T_{uc}$. Therefore, the probability density function for the time it takes one MT to capture one kinetochore in the biased model is exponential: $P(t \le \tau) \approx 1 - e^{-p\tau/T_{uc}}$, exactly as in the biased model (Equation S9), where, however, T_{uc} and p are different. The analysis of the unbiased model above is then immediately applicable to the biased model. Namely, for N_M MTs and N_K kinetochores:

$$T^{N_M,N_K}_{search}(biased) = C\frac{T_{uc}(biased)}{N_M p(biased)} \ln N_K,$$

$$\sigma(biased) \approx 1.3 \cdot \frac{T_{uc}(biased)}{N_M p(biased)},\ C \sim 1 \quad \text{(S19)}$$

Similarly, the corresponding probability density function is given by Equation S15 and has the same shape as it does for the unbiased model.

Dependence of the Average Search Time on the Kinetochore Radius and MT Number

The time to capture is inversely proportional to the number of searching MTs and to the square of the kinetochore radius. Therefore:

$$r_{kt} = A/\sqrt{N_M} \quad \text{(S20)}$$

where A is an arbitrary constant that gives the level curves of search time in the $r_{kt} - N_M$ space.

Analysis of the Difference in Capture Time between the Unbiased and Biased Models

Equations S17 and S19 show that the average time until capture in the biased model is less than that in the unbiased model by a factor equal to $[p(biased)/p(unbiased)] \cdot [T_{uc}(unbiased)/T_{uc}(biased)]$. The directional factor is the same in both models, but in the biased model there is no chance for a MT to catastrophe before reaching the target, if we assume the piecewise constant catastrophe rate, whereas in the unbiased model the respective event decreases the number of successful MTs by approximately 2.7 in the optimal case. Therefore, $p(biased)/p(unbiased) \sim 2.7$. Half of the MTs in the biased model—those growing in the "wrong" direction, away from the sphere of the nucleus—catastrophe immediately, thereby decreasing the ratio $T_{uc}(unbiased)/T_{uc}(biased)$ by a factor of 2. Furthermore, in the unbiased model, MTs have to grow equally long on average, independently of their orientation. On the contrary, in the biased model, MTs growing in a direction almost normal to the straight line between the spindle poles reach the edge of the nuclear sphere quickly and catastrophe. Because of that, the average length of the searching MTs is much smaller in the biased model. The numerical analysis described below predicts that in the biased model the MTs are on the average 1.7 times shorter (so the corresponding cycle time is 1.7 times shorter) than those in the unbiased case. Therefore, $T_{uc}(unbiased)/T_{uc}(biased) \sim 2 \times 1.7 = 3.4$ and

$$T^{N_M,N_K}_{search}(unbiased)/T^{N_M,N_K}_{search}(biased) \sim 2.7 \times 3.4 = 9.2, \quad \text{(S21)}$$

so the analysis predicts that the search and capture time in the biased model is an order of magnitude smaller than it is in the biased model.

Computer Simulations of the Search-and-Capture Process

The practical use of the mathematical analysis is limited because:

(1) The kinetochores are distributed in a specific way, and formulae for computing probability distributions and averages become too cumbersome when kinetochore location is taken into account;
(2) In the biased model, the unsuccessful search time is not an exponential random variable, so it is not possible to derive the exact probability distribution for the sum of the unsuccessful search times;
(3) Most importantly, the approximations in the analysis above are valid in the limit when the typical search requires several repeated attempts (multiple nucleation events: $pN_M \le 1$. However, when the total MT number is large, this is not always true. For example, in the biased model, if

$$N_M = 500,\ r_k = 1\ \mu m,\ x = 10\ \mu m,\ pN_M \sim (r_k^2 N_M/4x^2) \sim 1,$$

and the error of the approximation becomes too great.

Therefore, we use Monte Carlo simulations as follows.

I. Optimal catastrophe frequency in the unbiased model

Equation S11 gives the optimal catastrophe frequency in the case of one kinetochore at distance x. In the case of many kinetochores randomly positioned within the nuclear sphere, the optimal frequency depends on a weighted average of the average time to capture. First, because each kinetochore has to be captured from both poles, we generated 10^6 random positions of kinetochores uniformly distributed inside the nuclear sphere and calculated numerically the distance from both poles generating $2 \cdot 10^6$ random distances. We used this set of distances to estimate numerically the probability density function of pole-kinetochore distances. Second, we used a random number generator to generate a few dozen catastrophe frequency values and a few dozen values of x, the latter by using the computed probability density function of pole-kinetochore distances. Third, we found the average weighted search time for each frequency by using Equation S10 to find the search time for each distance and then calculating the average. Finally, we numerically found the optimal catastrophe frequency that minimizes this weighted average time for capture.

The result is

$$f_{cat}^{optimal} \approx 0.0134/\text{sec}. \qquad \text{(S22)}$$

The corresponding average MT length found is $V_g/f_{cat}^{optimal}$:

$$\langle x \rangle(unbiased) = V_g/f_{cat}^{optimal} \approx 13.3\ \mu\text{m}. \qquad \text{(S23)}$$

In the biased sphere model, we used the same computed probability density function of pole-kinetochore distances to find the average MT length. If we count only MTs that grow in the nuclear sphere, this average is close to 8 μm. However, half of the MTs—those growing away from the sphere—catastrophe immediately, bringing the average length down to

$$\langle x \rangle(biased) \approx 4\ \mu\text{m}. \qquad \text{(S24)}$$

II. Simulation of the time to capture in the unbiased model

The computer code works as follows:

1. Chromosome positions are generated randomly within the nuclear sphere, and two corresponding pole-kinetochore distances are calculated.
2. For each of these distances, the probability of a successful search, p, is calculated from Equation S4.
3. The number n of unsuccessful searches is generated randomly according to the geometric probability distribution: $P(n) = p(1 - p)^n$.
4. The duration of each unsuccessful search is generated randomly according to the exponential probability distribution $P(t) \sim \exp(-t/T_{uc})$, where T_{uc} is given by Equation S5 and the sum of n such times, plus the successful search time (x/V_g), is calculated.
5. The previous four steps are repeated N_M (number of MTs) times for each of the chromosomes, then $(N_K/2)$ (number of chromosomes) times.
6. The maximum of N_K search times is found; this is the search time of one numerical experiment.
7. A large number of numerical experiments (the first six steps) are carried out, and the results are reported in the histograms and processed statistically.

III. Simulation of the time until capture in the biased model with the sphere of influence

The computer code works as follows:

1. Chromosome position is generated randomly within the nuclear sphere, and two corresponding pole-kinetochore distances are calculated.
2. For each of these distances, the probability of a successful search is calculated from the formula $p = r_{kt}^2/(4x^2)$.
3. The number n of unsuccessful searches is generated randomly according to the geometric probability distribution: $P(n) = p(1 - p)^n$.
4. The duration of each unsuccessful search is generated randomly, first by finding a random MT length X_i according to the computed probability density function of "pole to edge of the nucleus," and then by finding the corresponding time $T_i = X_i \cdot (1/V_g) + (1/V_s)]$. Then, the sum of n such times, plus the successful search time (x/V_g), is calculated.
5. The previous four steps are repeated N_M (number of MTs) times for each of the chromosomes, and then $(N_K/2)$ (number of chromosomes) times.
6. The maximum of N_K search times is found—this is the search time of one numerical experiment.
7. A large number of numerical experiments (the first six steps) are carried out, and the results are reported in the histograms and processed statistically.

IV. Simulation of the time until capture in the biased model with continuous spatial RanGTP gradient

The computer code works as follows:

1. Positions of 46 chromosomes are generated randomly and uniformly within the nuclear sphere.
2. The spatial RanGTP distribution is generated as a linear superposition of the exponentially decreasing [S6] concentrations of RanGTP centered at each kinetochore:

$$Ran(\vec{x}) = A\sum_{i=1}^{46} e^{-\gamma_1|\vec{x}-\vec{x}_i|},$$

   where A is the RanGTP concentration in the immediate vicinity of a chromosome and γ_1 is the inverse space constant associated with the decay RanGTP away from a kinetochore. RanGTP spreads effectively from a chromosome, $\vec{x}$ is the 3-D coordinate, and $\vec{x}_i$ is the coordinate of the center of i^{th} kt. (The exact value of A is irrelevant provided it is sufficiently large; the order of magnitude of the parameter γ_1 is 1/(a few μm)—numerical experiments showed that fine tuning of this parameter does not affect the results.)
3. The spatially dependent catastrophe frequency was calculated as

$$f_{cat}(\vec{x}) = B\ \exp(-\gamma_2 Ran(\vec{x})),$$

   where γ_2 is a phenomenological parameter showing how sensitive the catastrophe frequency is to RanGTP concentration and B is the maximal fre-

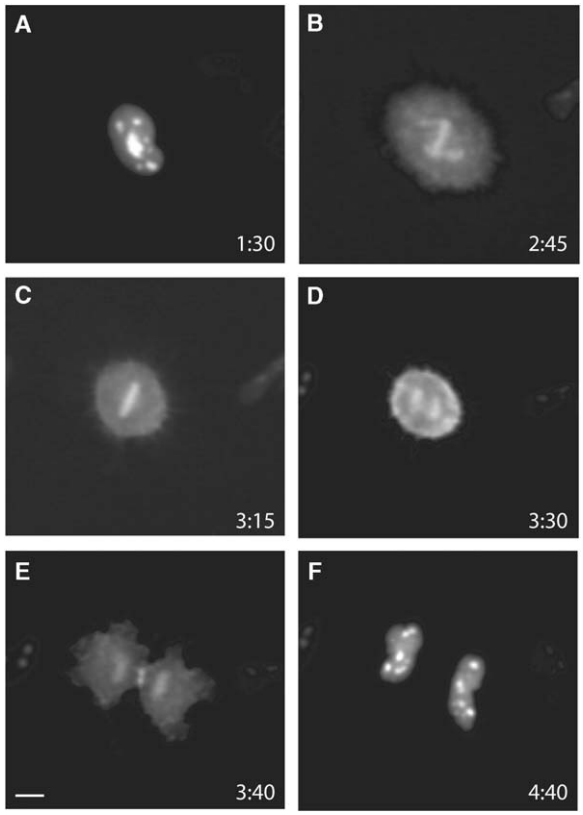

Figure S1. Mitosis Time Measured with the Mitosis Biosensor

During interphase (A) the florescence biosensor is localized to the nucleus. After NEB and during prometaphase (B), the biosensor has a diffusive cytosolic localization pattern as well as an electrostatic ionic interaction with the condensed chromatids; this interaction allows for the visualization of the metaphase plate (C) and sister-chromatid separation during anaphase (D). Finally, cytokinesis (E) and the reformation of the nuclear envelope in two daughter cells (F) mark the end of mitosis. The scale bar represents 5 μm.

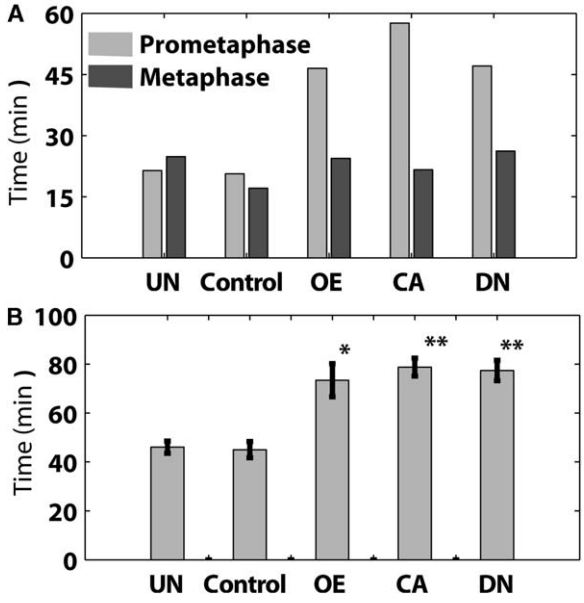

Figure S2. Duration of Different Stages of Mitosis in Cells Expressing Different Forms of Ran

Measurement of prometaphase and metaphase (A) and NEB until anaphase duration (B) in untransfected cells (UN); control cells transfected with CFP (control); cells overexpressing native Ran (OE); cells expressing a constitutively active mutant form of Ran (CA); and cells expressing a dominant-negative mutant (DN) form of Ran. * p value $<10^{-5}$, ** p value $<10^{-8}$ in a comparison to untransfected cells via a Student's t test. Error bars are standard error (SEM). The total numbers of mitotic cells measured were 35, 49, 22, 66 and 42 for control, UT, OE, CA, and DN, respectively. Out of these, congression was visible in 31, 47, 17, 27, and 11 cells, respectively, and both prometaphase and metaphase duration were measured.

quency. The phenomenological function $f_{cat}(\vec{x})$ is chosen so that at high (low) RanGTP concentration the catastrophe frequency tends to zero (maximum). (The exact value of B is irrelevant provided it is sufficiently large; we varied the value of the parameter γ_2 in the numerical experiments. The results are not sensitive to specific functional dependence of the catastrophe rate on RanGTP concentration; linear dependence works as well as the exponential one.)

4. RanGTP concentrations and corresponding catastrophe frequency distributions $f^i_{cat}(l)$ along the trajectories from each pole to the 46 corresponding kinetochores were calculated from the 3-D RanGTP distribution with 3-D linear interpolation in Matlab.
5. For each kinetochore, the probability of a successful search is calculated with numerical integration applied to the formula $p = r_{kt}^2/(4x^2) \cdot P_{no\ cat}$ where

$$P_{no\ cat} = \exp\left(-\int_0^x f^i_{cat}(l)dl/V_g\right).$$

6. The number n of unsuccessful searches is generated randomly according to the geometric probability distribution: $P(n) = p(1-p)^n$.
7. The duration of each unsuccessful search is generated randomly, along a randomly generated trajectory, by (i) finding the catastrophe frequency distribution $f^i_{cat}(l)$ along this trajectory, (ii) finding the random maximal MT length X_i (via the inverse method for random number generation for a non-homogeneous Poisson process [S1]) characterized by the probability density

$$\sim\exp\left(-\int_0^{x_i} f^i_{cat}(l)dl/V_g\right),$$

and (iii) finding the corresponding time $T_i = X_i \cdot [(1/V_g) + (1/V_s)]$. Then, the sum of n such times, plus the successful search time (x/V_g), is calculated.
8. The previous seven steps are repeated for all kinetochores.
9. The maximum of the search times is found—this is the search time of one numerical experiment.

To save computation time, a "shortcut" was used, such that when the number of unsuccessful nucleations was greater than 50, the time until capture was approximated by a normal distribution for which the average and variance were calculated based on 500 random-nucleation cycles. Even with this shortcut, a single nu-

Table S1. Terms Used in This Study

Symbol	Meaning	Type	Value/Distribution/Equation
t	Time until capture	Random Variable	Equations S9, S12, S15
n	Number of nucleation cycle needed until a successful one for a single MT	Random Variable	Geometric discrete
p	Probability for single MT to capture target	Random Variable	Depends on x, r_{kt}, f_{cat}, V_g see Equation S4
x	Pole-kinetochore distance	Random Variable	Uniform in sphere radius r_{nuc}
T_s	The time it takes a MT to grow to the distance x	Random Variable	$T_s = x/V_g$
$T^{i,j}_{search}$	Time for i MTs to capture j kinetochores (targets)	Random Variable	Equations S10, S13, S17, and S19
σ	Standard deviation of search time	Random Variable	Equation S18
$P_{direction}$	Probability to nucleate in the right direction toward a target	Random Variable	Equations S2
$P_{no\ cat}$	Probability not to catastrophe before reaching the target	Random Variable	Equations S3
T_{uc}	Average time of an unsuccessful nucleation cycle	Variable	Equations S5
f_{rescue}	MTs Rescue frequency	Optimized Parameter	0 [1/s]
f_{cat}	MTs Catastrophe frequency	Optimized Parameter	0.0134 [1/s]
N_M	Number of searching MTs	Parameter	250 / 1000 (see Fig 3.)
N_K	Number of kinetochore (targets)	Parameter	92
r_{nuc}	Radius of the nucleus	Parameter	10 [μm]
r_{kt}	Effective radius of the kinetochore	Parameter	0.44 [μm] (see Fig. 3)
V_s	MT shrinking velocity	Parameter	0.2050 [$\mu m/s$]
V_g	MT growth velocity	Parameter	0.1783 [$\mu m/s$]

merical experiment took longer than 24 hr on an IBM dual CPU Opteron server. Therefore, we could not gather enough statistics from simulations of this sophisticated model. However, with a limited number of numerical experiments, we established that:

1. The average capture time is a decreasing function of γ_2 (within certain limits). This means that the more sensitive catastrophe frequencies are to RanGTP concentration, the more efficient is kinetochore capture. Note that large values of γ_2 generate a catastrophe frequency distribution that resembles the piecewise constant model described in III.
2. The times to capture were close to and slightly greater than those computed in the model where the catastrophe frequency is zero in the nuclear sphere and very large outside of it. Therefore, we conclude that the biased model with the sphere of influence is the optimal way to use the RanGTP gradient to guide MTs to capture kinetochores.

Model limitations: In the simulations, we neglected the effect of decreasing the number of searching MTs after part of the kinetochores is attached because the number of the searching MTs is typically an order of magnitude greater than the kinetochore number, and this effect does not introduce large error. We also neglect crosslinking of some of the searching MTs with their counterparts from the opposite pole. Note also that these errors would increase the effective search-and-capture time slightly, whereas our main focus is estimating the lower limit for this time.

A very difficult issue left to be dealt with in the future is that history dependence in MT dynamic instability could play an important role in animal-cell chromosome capture; it has been shown that during their assembly in vitro [S7], in extracts [S8], and in interphase cells [S9], MTs exhibit history dependence in their catastrophe behavior. Specifically, it has been found that the distribution of growth times in vitro is γ distributed [S7] rather than exponential, as is generally assumed. If catastrophe is low early in the growth phase, then MTs will tend to persist out to the edge of the nuclear sphere, thereby increasing the probability not to catastrophe until attachment. (This effect was considered in [S6] in a different context.)

Supplemental Experimental Procedures and Results

Hela cells constitutively expressing the fluorescent mitosis biosensor [S5] were grown in Dulbecco's modified Eagles medium (DMEM) supplemented with 10% fetal calf serum, 2 mM glutamine, 100 U/ml penicillin, and 100 μg/ml streptomycin (from Invitrogen). Hela cells (2500) were plated in 96-well polystyrene plates (Costar) and 24 hr later were transfected with 1 μl of Fugene (Roche) and 400 ng of the following constructs, ECFP (Clontech), wild-type Ran fused to ECFP, constitutively active Ran (RanQ69L) fused to ECFP or the dominant-negative Ran (RanL43E) fused to CFP. Ran constructs were gifts of Won Do Heo [S10]. Because of the toxicity of the Ran constructs, imaging was started 10 hr after transfection. The cells were imaged with an Axon ImageXpress 5000A equipped with an environmental control system (Molecular Devices). The imaging chamber was maintained at 37°C and 5% CO_2. Cells were imaged with a framing rate of every 5 min for the EYFP and every 30 min for the ECFP with a 10× objective lens for approximately 12 hr. Images were compiled into sequences with the IXconsole (Molecular Devices), and mitotic cells were analyzed. NEB was determined as the time the mitosis biosensor redistributed from the nucleus throughout the cell. As can be seen from Figure S1, the biosensor clearly localizes to condensed chromatin, allowing prometaphase, metaphase, and anaphase to be identified; e.g., at metaphase the chromatin-associated biosensor was aligned in one plane in the middle of the cell. Figure S2 shows the prometaphase and metaphase durations measured in the wild-type and mutant cells.

Theoretical Procedures

The numerical codes were implemented with Matlab. Numerical experiments were performed on an IBM dual CPU Opteron server.

Supplemental References

S1. Sokolnikoff, I.S., and Redheffer, R.M. (1966). Mathematics of Physics and Modern Engineering. (New York: McGraw-Hill)

S2. Howard, J. (2001). Mechanics of Motor Proteins and the Cytoskeleton (Sunderland, MA: Sinauer).
S3. Ross, S.M. (1972). Introduction to Probability Models. (New York: Academic Press).
S4. Holy, T.E., and Leibler, S. (1994). Dynamic instability of microtubules as an efficient way to search in space. Proc. Natl. Acad. Sci. USA 91, 5682–5685.
S5. Jones, J.T., Myers, J.W., Ferrell, J.E., and Meyer, T. (2004). Probing the precision of the mitotic clock with a live-cell fluorescent biosensor. Nat. Biotechnol. 22, 306–312.
S6. Sprague, B.L., Pearson, C.G., Maddox, P.S., Bloom, K.S., Salmon, E.D., and Odde, D.J. (2003). Mechanisms of microtubule-based kinetochore positioning in the yeast metaphase spindle. Biophys. J. 84, 3529–3546.
S7. Odde, D.J., Cassimeris, L., and Buettner, H.M. (1995). Kinetics of microtubule catastrophe assessed by probabilistic analysis. Biophys. J. 69, 796–802.
S8. Dogterom, M., Felix, M.A., Guet, C.C., and Leibler, S. (1996). Influence of M-phase chromatin on the anisotropy of microtubule asters. J. Cell Biol. 133, 125–140.
S9. Howell, B., Odde, D.J., and Cassimeris, L. (1997). Kinase and phosphatase inhibitors cause rapid alterations in microtubule dynamic instability in living cells. Cell Motil. Cytoskeleton 38, 201–214.
S10. Heo, W.D., and Meyer, T. (2003). Switch-of-function mutants based on morphology classification of Ras superfamily small GTPases. Cell 113, 315–328.
S11. Rusan, N.M., Tulu, U.S., Fagerstrom, C., and Wadsworth, P. (2002). Reorganization of the microtubule array in prophase/prometaphase requires cytoplasmic dynein-dependent microtubule transport. J. Cell Biol. 158, 997–1003.